Nucleon resonance contributions to unpolarised inclusive electron scattering

A. N. Hiller Blin,[1] V. Mokeev,[2] M. Albaladejo,[2] C. Fernández-Ramírez,[3]
V. Mathieu,[2] A. Pilloni,[4,5] and A. Szczepaniak[2,6]
(Joint Physics Analysis Center)

V. D. Burkert,[2] V. V. Chesnokov,[7] A. A. Golubenko,[7] and M. Vanderhaeghen[1]

[1] *Institut für Kernphysik & PRISMA$^+$ Cluster of Excellence, Johannes Gutenberg Universität, D-55099 Mainz, Germany*
[2] *Thomas Jefferson National Accelerator Facility, Newport News, VA 23606, USA*
[3] *Instituto de Ciencias Nucleares, Universidad Nacional Autónoma de México, Ciudad de México 04510, Mexico*
[4] *European Centre for Theoretical Studies in Nuclear Physics and related Areas (ECT*) and Fondazione Bruno Kessler, Villazzano (Trento), I-38123, Italy*
[5] *INFN Sezione di Genova, Genova, I-16146, Italy*
[6] *Center for Exploration of Energy and Matter, Indiana University, Bloomington, IN 47403, USA*
[7] *Skobeltsyn Nuclear Physics Institute and Physics Department at Moscow State University, 119899 Moscow, Russia*

(Dated: Friday 5$^{\text{th}}$ April, 2019)

The first CLAS12 experiments will provide high-precision data on inclusive electron scattering observables at a photon virtuality Q^2 ranging from 0.05 GeV^2 to 12 GeV^2 and center-of-mass energies W up to 4 GeV. In view of this endeavour, we present the modeling of the resonant contributions to the inclusive electron scattering observables. As input, we use the existing CLAS electrocoupling results obtained from exclusive meson electroproduction data off protons, and evaluate for the first time the resonant contributions based on the experimental results on the nucleon resonance electroexcitation. The uncertainties are given by the data and duly propagated through a Monte Carlo approach. In this way, we obtain estimates for the resonant contributions, important for insight into the nucleon parton distributions in the resonance region and for the studies of quark-hadron duality.

I. INTRODUCTION

Studies of inclusive electron scattering off nucleons represent an important avenue in the exploration of the nucleon structure. The global analysis [1–5] (see also the reviews in Refs. [6–8]) has delivered detailed information on the parton distribution functions of the nucleon (PDFs) for all quark flavors and gluons in the Bjorken variable range of $10^{-4} < x < 1$. In particular, the Jefferson Lab inclusive electron scattering data [9–12] had a major impact on the contemporary knowledge of the PDFs contributing to the large-x data in the nucleon resonance region [9, 13, 14]. Due to its near 4π angular coverage, the CLAS detector offers a unique possibility of obtaining the inclusive structure functions $F_2(x, Q^2)$ in a very broad range of x (or W) at a given photon virtuality Q^2. This is particularly important in the resonance region, due to the presence of several resonant structures in the observable kinematics, which makes it challenging to use the typical interpolation of $F_2(x, Q^2)$ structure functions over x at fixed Q^2. A compilation of the data for the unpolarized structure functions and inclusive cross sections together with a tool for the interpolation between bins is available online from the CLAS database [15–17]. This tool covers the range 1.07 GeV $\leq W \leq$ 4 GeV and 0.5 GeV^2 $\leq Q^2 \leq$ 7 GeV^2. It uses the data and fits thereof [9, 11] for the interpolation and extrapolation to regions outside the data coverage. The structure function $F_1(x, Q^2)$ was obtained from the data on $F_2(x, Q^2)$, assuming the parametrization in Ref. [9, 18] for the longitudinal over transverse cross section ratio R_{LT}. In this work, we update R_{LT} to the more recent parametrization described in Ref. [19], based on data from the ZEUS and H1 experiments [20–22]. The online tool is particularly useful for the analyses of the CLAS12 experiments, which will achieve the largest ever Q^2 coverage in the resonance region, also for the inclusive data [23].

There is a strong interest in studying the structure functions at large x within the resonance region, since this range is dominated by the contributions from the valence quarks and there are several theoretical predictions for the PDF's in the limit of $x \to 1$ that need to be validated [24–28]. Furthermore, recent developments of novel approaches to PDFs using Euclidean concepts [29–32] make it possible to calculate in lattice QCD quantities that should converge to the measured PDFs. The PDFs in the resonance region were also evaluated with the help of quark-hadron duality [10, 33–36], which relates the inclusive structure functions averaged over individual resonance widths to the continuum evaluated using the deep inelastic scattering (DIS) region. Quark-hadron duality has been shown to approximately work even at Q^2 as low as 1 GeV^2 [10].

In the past years, the CLAS experiments on exclusive meson electroproduction [37–43] coupled with sophisticated analysis models [44–49] enabled to determine individual nucleon resonance contributions to electroproduction by measuring, for the first time, nucleon resonance transverse $A_{1/2}$, $A_{3/2}$ and longitudinal $S_{1/2}$ electroexcitation amplitudes (also refered to as the $\gamma_v pN^*$ electrocouplings).

As of now, the photocouplings of most of the excited

nucleon states in the mass range up to 2 GeV have been well determined [50, 51]. On the other hand, the $\gamma_v pN^*$ electrocouplings in the mass range up to 1.8 GeV were determined by CLAS for a Q^2 range up to 5.0 GeV^2 from the $N\pi$ [38, 46], $N\eta$ [52–54] and $\pi^+\pi^- p$ [45, 47, 48] channels, and have been made available online [55]. The consistency of the results in the different channels supports their extraction [48]. In addition, substantial evidence of a new baryon state $N'(1720)$ $3/2^+$ has been found recently [39, 43]. The electrocouplings of nucleon resonances in the 1.8–2.0 GeV mass range and at 0.4 GeV^2 $< Q^2 <$ 5.0 GeV^2 will soon become available from data [56–59]. With the CLAS12 endeavour, the Q^2 coverage is to be extended to the largest interval ever achieved in exclusive reaction studies, from 0.05 GeV^2 to 12 GeV^2. The aim is also to explore the high-lying resonances at $W > 2.0$ GeV, so as to include the search for new states of hadron matter, the so-called hybrid baryons with glue as active constituents [60, 61]. In the Spring of 2018, the first experiments with the CLAS12 detector have already run successfully [23].

It is of ever growing importance to consistently include the effects of the resonant and non-resonant (background) contributions into a single framework. This is possible with a combined study of exclusive and inclusive electron scattering data: the exclusive reactions offer us insight into the Q^2 evolution of the resonance electrocouplings; these can then be used as input for the computation of the resonant contributions to the inclusive cross sections.

The availability of $\gamma_v pN^*$ electrocoupling data on individual nucleon resonances makes it possible to evaluate the resonant contributions to the inclusive electron scattering observables, which is the goal of the present work. We use a relativistic Breit-Wigner ansatz to estimate the resonant contributions to the inclusive electron-scattering unpolarized cross sections, which relate to the unpolarized structure functions. As input, the known masses and widths of the resonances are used, as well as the experimental information on electrocouplings from CLAS. This allows us to single out the resonant contributions to the inclusive electron scattering observables. We emphasize that this information is obtained from the exclusive meson electroproduction data off protons and is independent of the inclusive measurements. Therefore, it can also be used to estimate the non-resonant part of the inclusive electron scattering. As one moves towards higher W (lower x) this will allow in a next step to determine the transition between resonant and non-resonant contributions and consequently between resonance bound valence quarks and asymptotically free partons. The results of the present work are very timely, since with the CLAS12 experiments the input from exclusive reactions will be extended further, and at the same time more data will be available on inclusive reactions, with higher precision and within nearly 4π acceptance.

The rest of the paper is organized as follows. In Sec. II, we discuss the formalism on using exclusive reactions to estimate the resonant contributions to inclusive electron scattering. We show the results for the resonant contributions to the structure function F_2 from the inclusive CLAS data in Sec. III. There, we also show the resonant contributions to the transverse, longitudinal and unpolarized full inclusive cross sections, which in the present framework can be duly evaluated from the transverse and longitudinal $\gamma_v pN^*$ electrocoupling values without the need of parametrizing R_{LT}. In Sec. IV, we summarize our findings and discuss their applicability, also in view of the upcoming experimental results.

II. FORMALISM

In order to describe the contributions of the N^* and Δ^* resonances to the observables in inclusive $e^- p$ scattering, we include the information on the $\gamma_v pN^*$ electrocouplings of the resonances with masses below 1.8 GeV from CLAS [55, 62]. Apart from the resonances whose existence is certain (marked as four stars in the Review of Particle Physics (RPP) [63]), we include the new $N'(1720)$ $3/2^+$ state [39, 43], since the used CLAS electrocouplings were obtained accounting for its contribution. The resonances and their properties, as used in this work, are listed in Table I.

N^*	M_r [MeV]	Γ_r [MeV]	L_r	$\beta_{\pi N}$	$\beta_{\eta N}$	$\beta_{r.}$	X [GeV]
$\Delta(1232)$ $3/2^+$	1232	117	1	1.00	0	0	—
$N(1440)$ $1/2^+$	1430	350	1	0.65	0	0.35	0.3
$N(1520)$ $3/2^-$	1515	115	2	0.60	0	0.40	0.1
$N(1535)$ $1/2^-$	1535	150	0	0.45	0.42	0.13	0.5
$\Delta(1620)$ $1/2^-$	1630	140	0	0.25	0	0.75	0.5
$N(1650)$ $1/2^-$	1655	140	0	0.60	0.18	0.22	0.5
$N(1675)$ $5/2^-$	1675	150	2	0.40	0	0.60	0.5
$N(1680)$ $5/2^+$	1685	130	3	0.68	0	0.32	0.2
$\Delta(1700)$ $3/2^-$	1700	293	2	0.10	0	0.90	0.22
$N(1710)$ $1/2^+$	1710	100	1	0.13	0.30	0.57	0.5
$N(1720)$ $3/2^+$	1748	114	1	0.14	0.04	0.82	0.5
$N'(1720)$ $3/2^+$	1725	120	1	0.38	0	0.62	0.5

Table I. Values used for resonance masses, widths, branching fractions β and quantum numbers, based on the RPP [63], with modifications to the $N(1720)$ $3/2^+$ and $\Delta(1700)$ $3/2^-$ states due to the inclusion of the new $N'(1720)$ $3/2^+$ state. See the text for discussion of the residual branching fractions β_r. The values of the inverse radii X for each resonance are also shown, following Refs. [44, 49].

The resonant contributions to the transverse (σ_T^R) and

longitudinal (σ_L^R) inclusive virtual photon-proton cross sections from a resonance of mass M_r, total width at the resonant point $\Gamma_r = \Gamma_{\rm tot}(W = M_r)$ and spin J_r can be described using the Breit-Wigner formula [47]

$$\sigma^R_{T,L}(W,Q^2) = \frac{\pi}{q^2_\gamma} \times \sum_{N^*}(2J_r+1)\frac{M_r^2\Gamma_{\rm tot}(W)\Gamma_\gamma{}^{T,L}(M_r,Q^2)}{(M_r^2-W^2)^2+M_r^2\Gamma^2_{\rm tot}(W)}, \quad (1)$$

with the following kinematics

$$\begin{aligned} q_\gamma &= \sqrt{Q^2+E^2_\gamma}, \\ E_\gamma &= \frac{W^2-Q^2-M_N^2}{2W}, \\ K &= \frac{W^2-M_N^2}{2W}. \end{aligned} \quad (2)$$

Here E_γ and q_γ are the virtual photon energy and magnitude of its three-momentum in the center-of-mass frame, respectively, and K is the equivalent photon energy. As usual, $q^2 = -Q^2$ is the 4-momentum squared of the virtual photon, while W is the virtual photon-proton system's center-of-mass energy. The resonance electromagnetic decay widths to the final states with transversely (Γ^T_γ) and longitudinally (Γ^L_γ) polarized photons at the resonant point are given by

$$\begin{aligned} \Gamma^T_\gamma(W=M_r,Q^2) &= \frac{q^2_{\gamma,r}(Q^2)}{\pi}\frac{2M_N}{(2J_r+1)M_r} \\ &\quad \times \left(|A_{1/2}(Q^2)|^2+|A_{3/2}(Q^2)|^2\right), \\ \Gamma^L_\gamma(W=M_r,Q^2) &= 2\frac{q^2_{\gamma,r}(Q^2)}{\pi}\frac{2M_N}{(2J_r+1)M_r}|S_{1/2}(Q^2)|^2, \end{aligned} \quad (3)$$

with $q_{\gamma,r} = q_\gamma|_{W=M_r}$. The electrocouplings $A_{1/2}(Q^2)$, $A_{3/2}(Q^2)$ and $S_{1/2}(Q^2)$ are taken from the CLAS results listed in [55, 62]. For consistency with the electrocoupling normalization, the electrocouplings of the $\Delta(1620)$ $1/2^-$, $\Delta(1700)$ $3/2^-$, $N(1720)$ $3/2^+$ and $N'(1720)$ $3/2^+$ resonances, extracted from double-pion electroproduction off protons, need to include an additional factor q_γ/K in both the electromagnetic widths of Eq. 3, and a factor $1/2$ in the longitudinal width.

In order to compute the energy dependence of the resonance total decay width, we split it into three pieces, to take into account the decays into the two main two-body channels, πN and ηN, and the remainder, which includes $\pi\pi N$ and all other final states. The hadronic decay widths to these final states at the resonant points are computed as the products of the total decay widths from the RPP [63] and the respective branching fractions β, summarized in Table I. For the resonance decays into the πN and ηN final states, we use the central values of the respective branching fractions employed in the extraction of the $\gamma_v pN^*$ electrocouplings from exclusive πN electroproduction data [38, 46]. The branching fractions for the decays into the remaining channels $\beta_{\rm r.}$ are evaluated as

$$\beta_{\rm r.} = 1 - \beta_{\pi N} - \beta_{\eta N}. \quad (4)$$

For those resonances which decay preferentially into the $\pi\pi N$ final states, $\Delta(1620)$ $1/2^-$, $\Delta(1700)$ $3/2^-$, $N(1720)$ $3/2^+$, the values of $\beta_{\rm r.}$ obtained in this way are in good agreement with the branching fractions for resonance decays into the $\pi\pi N$ final states used in the extraction of the $\gamma_v pN^*$ electrocouplings from $\pi^+\pi^- p$ CLAS data [39, 40, 48]. Furthermore, as mentioned above, we include the new baryon state $N'(1720)$ $3/2^+$. It is needed in order to enable describing the data in the third resonance region such that the hadronic decay parameters are independent of Q^2. For this state, the branching fraction for the decay into the $\pi\pi N$ final state is available from the analysis of the CLAS data on $\pi^+\pi^- p$ electroproduction off protons [39]. We assume the remaining decay width for this resonance to be saturated by πN. In Eq. (1), the interference between different resonances is neglected. While this is correct when the resonances have different quantum numbers, and is a good approximation when the resonances are well separated, it needs further justification for the $N(1720)3/2^+$ and the $N'(1720)3/2^+$ of the same spin-parity and mass difference of only ≈ 25 MeV. Since the branching fractions for decays of these two resonances into $\pi\Delta$ and ρp final states are very different [39, 43], the effect is estimated to be lower than 10%, and will be neglected here.

The W-dependence of the total and partial resonance decay widths is determined by the centrifugal barrier penetration and can be parametrized as [44]

$$\Gamma_{\rm tot}(W) = \Gamma_{\pi N}(W) + \Gamma_{\eta N}(W) + \Gamma_{\rm r.}(W), \quad (5)$$

where

$$\begin{aligned} \Gamma_{\pi(\eta)N}(W) &= \Gamma_r\,\beta_{\pi(\eta)N} \\ &\quad \times \left(\frac{p_{\pi(\eta)}(W)}{p_{\pi(\eta)}(M_r)}\right)^{2L_r+1}\left(\frac{X^2+p_{\pi(\eta)}(M_r)^2}{X^2+p_{\pi(\eta)}(W)^2}\right)^{L_r}, \\ \Gamma_{\rm r.}(W) &= \Gamma_r\,\beta_{\rm r.} \\ &\quad \times \left(\frac{p_{\pi\pi}(W)}{p_{\pi\pi}(M_r)}\right)^{2L_r+4}\left(\frac{X^2+p_{\pi\pi}(M_r)^2}{X^2+p_{\pi\pi}(W)^2}\right)^{L_r+2}, \end{aligned} \quad (6)$$

and

$$\begin{aligned} p_{\pi(\eta)}(W) &= \sqrt{E^2_{\pi(\eta)}(W)-m^2_{\pi(\eta)}}, \\ E_{\pi(\eta)}(W) &= \frac{W^2+m^2_{\pi(\eta)}-M_N^2}{2W}, \\ p_{\pi\pi}(W) &= \sqrt{E^2_{\pi\pi}(W)-4m^2_\pi}, \\ E_{\pi\pi}(W) &= \frac{W^2+4m^2_\pi-M_N^2}{2W}. \end{aligned} \quad (7)$$

Note that an effective parametrization of the multibody decays is used [44]. The values of L_r are shown in Table I, as are the values of X, which are taken from the best fit in Refs. [44, 49]. An exception is made for the well-isolated $\Delta(1232)\ 3/2^+$ resonance, whose width is fully described by the πN decay in the following way [47]:

$$\Gamma_{\pi N}(W) = \Gamma_r \frac{M_r}{W} \frac{J_L^2[R\,p_\pi(M_r)] + N_L^2[R\,p_\pi(M_r)]}{J_L^2[R\,p_\pi(W)] + N_L^2[R\,p_\pi(W)]}, \quad (8)$$

where the interaction radius R was set to 1 fm. The functions J_L and N_L are the conventional Bessel and Neumann functions. In terms of the resonant electroproduction cross sections the unpolarized inclusive cross section is given by [11]

$$\sigma_U^R(W) = \sigma_T^R(W) + \epsilon_T \sigma_L^R(W), \quad (9)$$

$$\epsilon_T = \left(1 + 2\,\frac{\nu^2 + Q^2}{Q^2} \tan^2\frac{\theta_e}{2}\right)^{-1}, \quad (10)$$

where the electron scattering angle θ_e is written in terms of the electron beam energy E_b as

$$\sin^2\frac{\theta_e}{2} = \frac{Q^2}{4E_\mathrm{b}(E_\mathrm{b} - \nu)}, \quad (11)$$

and ν is the energy transferred by the virtual photon

$$\nu = \frac{W^2 - M_N^2 + Q^2}{2M_N}. \quad (12)$$

The transverse polarization parameter of the virtual photon ϵ_T is fully determined by the electron scattering kinematics. Comparing Eq. (9) with the standard definition of the structure functions one finally obtains [3, 32]

$$F_1^R(x, Q^2) = \frac{KW}{4\pi^2\alpha}\sigma_T^R(W, Q^2),$$
$$F_2^R(x, Q^2) = \frac{KW}{4\pi^2\alpha}\frac{2x}{1 + \frac{Q^2}{\nu^2}} \times \left[\sigma_T^R(W, Q^2) + \frac{Q^2}{\nu^2}\sigma_L^R(W, Q^2)\right], \quad (13)$$

where $x = \frac{Q^2}{2M_N\nu}$.

We use the interpolation/extrapolation tools developed by CLAS [62] for the central values of the electrocouplings. In order to estimate the uncertainties of the resonance contributions to the inclusive electron scattering observables, we interpolate between the error bars of the experimental bins in Q^2 [55]. As for the regions of Q^2 that are not covered by the resonance electrocoupling data, we assume the relative uncertainty to be the same as the one of the data point at highest Q^2. Note that this is only an extrapolation estimate, and therefore the results outside the data range in Q^2 need to be taken with care. Furthermore, the data for $\Delta(1620)1/2^-$, $N(1720)\ 3/2^+$, $N'(1720)\ 3/2^+$ and $\Delta(1700)\ 3/2^-$ cover a smaller range of $Q^2 < 1.5$ GeV^2 when compared to the other resonances, $Q^2 < 5$ GeV^2. For these resonances, we have preliminary estimates of the central electrocoupling values [43] based on the good description of the $\pi^+\pi^- p$ electroproduction data off protons from CLAS at 2.0 GeV^2 $< Q^2 <$ 5.0 GeV^2 [56, 58, 59]. We give a conservative extrapolation uncertainty estimate for these resonance electrocouplings of at least 20% (when the relative error as calculated above is smaller). The electrocoupling curves in the Q^2 range used in this work are shown in Figs. 1 to 3, and compared to electrocoupling world data [38, 39, 47, 48, 50, 52–54, 64–73].

For the propagation of the electrocoupling uncertainties to the observables, we use a bootstrap based approach. First, for each Q^2, resonance and electrocoupling type, we generate a set of values distributed as Gaussians according to their central value and error. The size of our set is of 10^4 samples, in order to obtain statistical significance. Then we use these 10^4 samples to generate 10^4 samples of the observables at each Q^2 and W value. The band of values within 1σ from the average value of these samples can then be determined.

III. RESULTS AND DISCUSSION

Within the approach described in Section II, we evaluate the resonant contributions to inclusive virtual photon-proton unpolarized cross sections and to their transverse and longitudinal parts, as well as to the inclusive structure function F_2, in the range 1.07 GeV $\lesssim W \lesssim$ 1.8 GeV that covers the three resonance regions. We also give predictions for inclusive electron scattering observables.

In Fig. 4, we display the central values of the transverse and unpolarized cross sections for different Q^2, decomposed into the contributions from each individual resonance. Although the resonances clearly cluster into three regions, one can see that each of them displays tails that give important contributions also to the neighboring regions. Therefore, a reliable extraction of the resonance parameters requires the analysis of the observables measured in a wide W interval overlapping with the neighboring resonance regions.

We first discuss the transverse cross section. The $\Delta(1232)\ 3/2^+$ represents a single contributor to the first resonance region, 1.07 GeV $\lesssim W \lesssim$ 1.4 GeV, but a tail from the $N(1440)\ 1/2^+$ also affects the cross section there at $Q^2 > 2.5$ GeV^2. Furthermore, it becomes increasingly relevant at higher Q^2, since the $\Delta(1232)\ 3/2^+$ electrocouplings decrease with Q^2 much faster than those of the $N(1440)\ 1/2^+$ [17].

The transverse resonant cross sections in the second resonance region, 1.4 GeV $\lesssim W \lesssim$ 1.6 GeV, are determined by the contributions from $N(1520)\ 3/2^-$, $N(1535)\ 1/2^-$ and the broad $N(1440)\ 1/2^+$. The contribution from the $N(1520)\ 3/2^-$ decreases with Q^2 faster

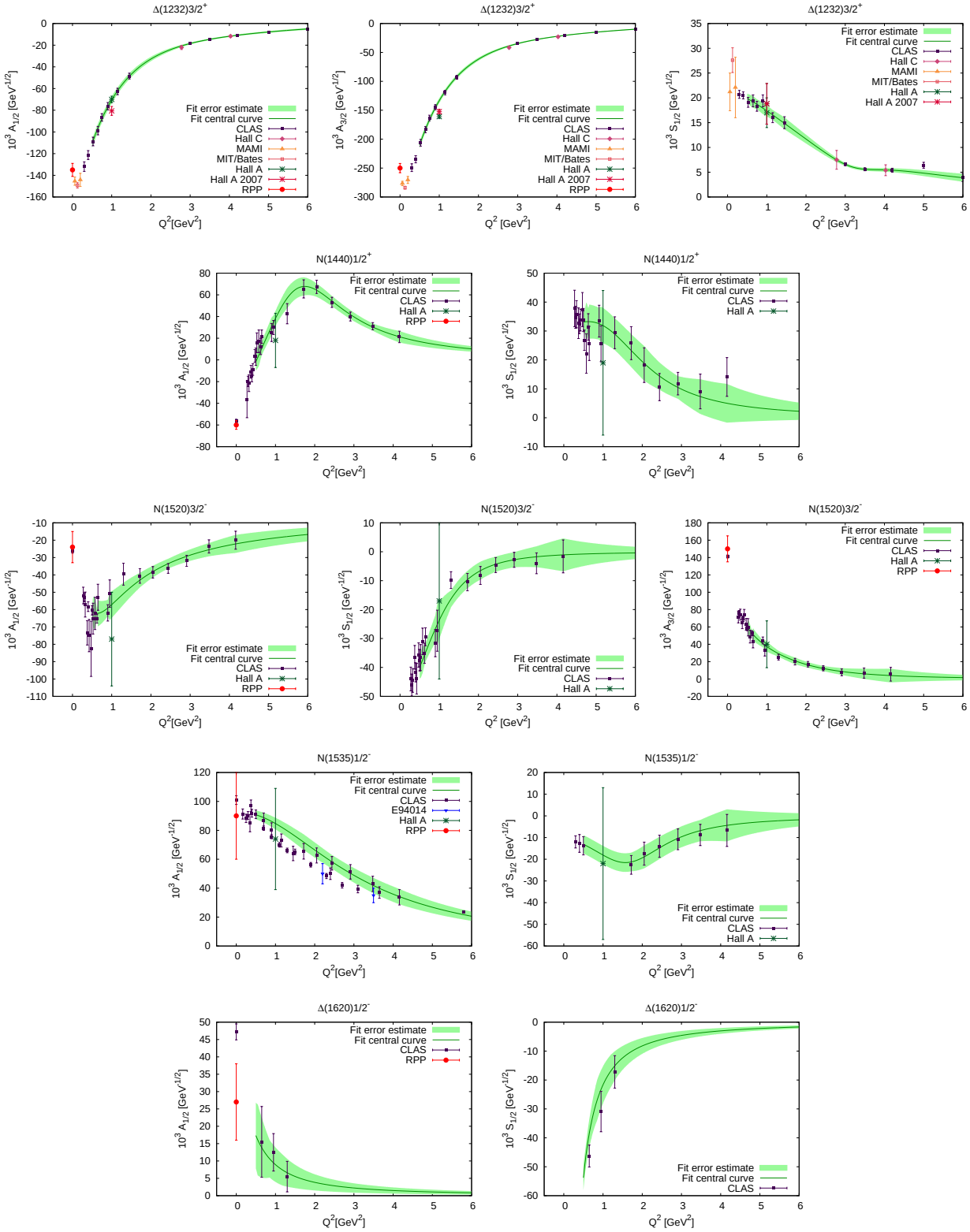

Figure 1. Electrocouplings of the $\Delta(1232)\ 3/2^+$, $N(1440)\ 1/2^+$, $N(1520)\ 3/2^-$, $N(1535)\ 1/2^-$ and $\Delta(1620)\ 1/2^-$. The left column shows $A_{1/2}$a nd the right column shows $S_{1/2}$, while the central column shows $A_{3/2}$ when applicable. The data are from the RPP [63], CLAS [47, 48, 50, 52–54, 72] the E94014 experiment [65], MAMI [69], MIT/Bates [67], Hall A [66, 68] and Hall C [70].

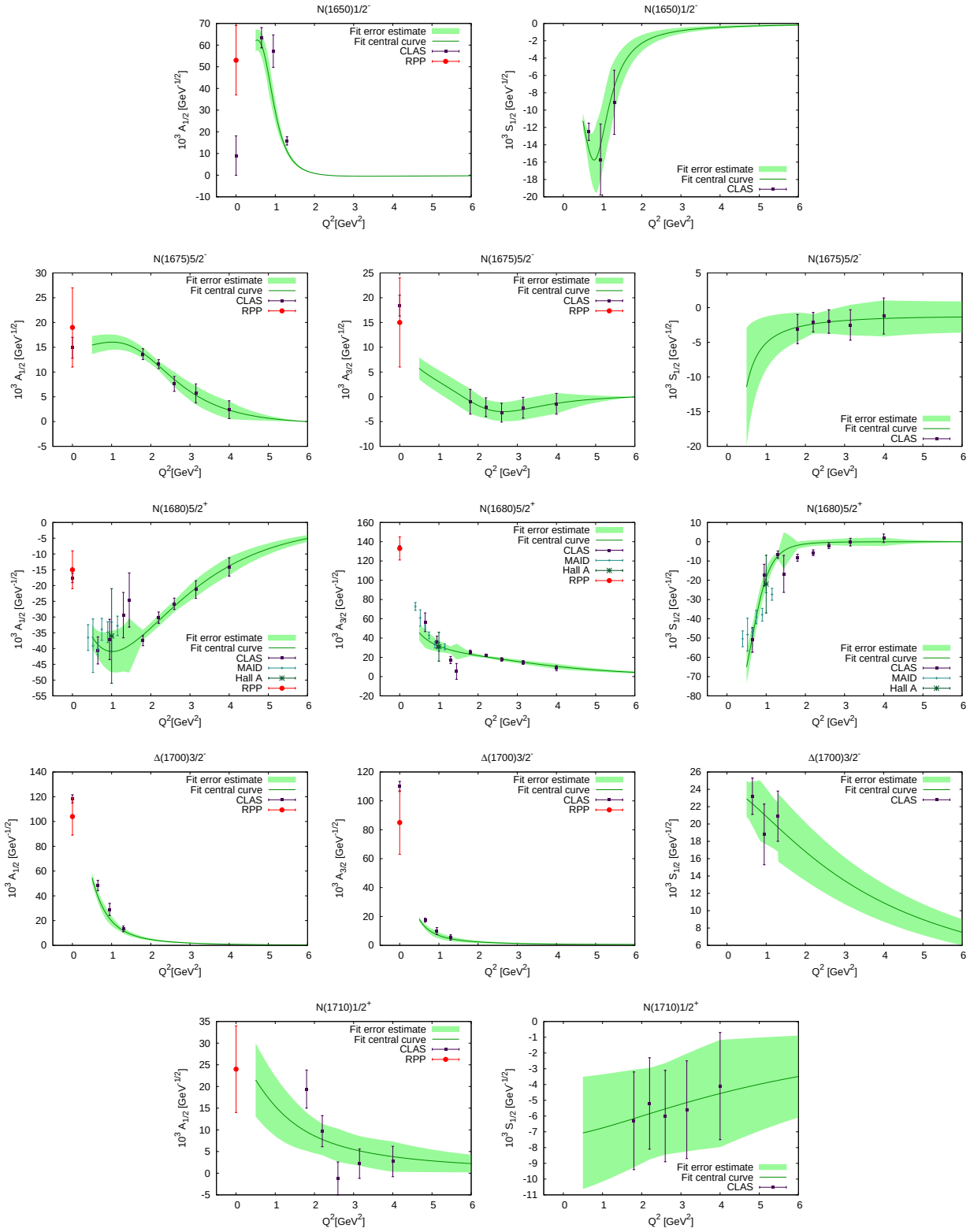

Figure 2. Electrocouplings of the $N(1650)\ 1/2^-$, $N(1675)\ 5/2^-$, $N(1680)\ 5/2^+$, $\Delta(1700)\ 3/2^-$ and $N(1710)\ 1/2^+$. The left column shows $A_{1/2}$ and the right column shows $S_{1/2}$, while the central column shows $A_{3/2}$ when applicable. The data points are from the RPP [63], CLAS [38, 50, 73], a MAID analysis [71] and Hall A [66].

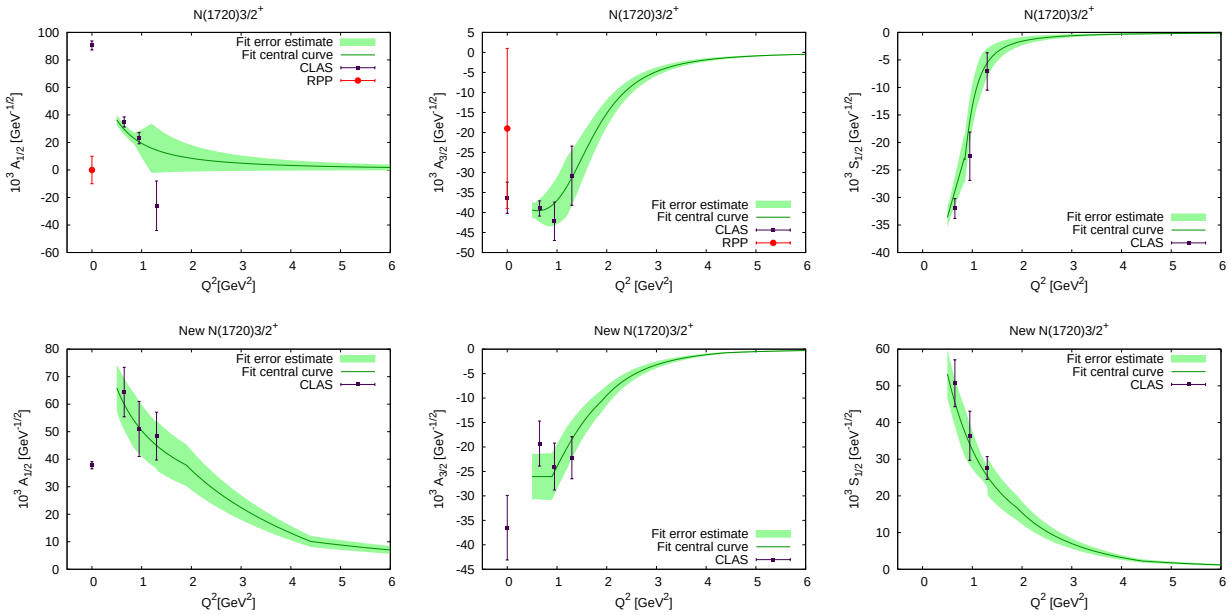

Figure 3. Electrocouplings of the $N(1720)\ 3/2^+$ and $N'(1720)\ 3/2^+$. The left column shows $A_{1/2}$a nd the right column shows $S_{1/2}$, while the central column shows $A_{3/2}$. The data points are from the RPP [63] and CLAS [39, 50].

than that from $N(1535)\ 1/2^-$, making the $N(1535)\ 1/2^-$ the largest contributor at $Q^2 > 2.0$ GeV^2. The slow decrease of the $N(1535)\ 1/2^-$ electrocouplings with Q^2 [55] results in an increase with Q^2 of its relative contribution to the transverse cross sections.

The third region, 1.6 GeV $\lesssim W \lesssim$ 1.8 GeV, is composed by several overlapping resonances, the largest contributions coming from the $N(1680)\ 5/2^+$ and the $N'(1720)\ 3/2^+$ candidate. The tail from the $N(1535)\ 1/2^-$ state becomes increasingly important in the generation of the resonant cross sections in the third resonance region at higher Q^2. Therefore, the knowledge on the electrocouplings of the $N(1535)\ 1/2^-$ in the second region plays an important role in describing the third region. The peak in the W-dependencies of the sum of contributions to the transverse cross sections at $W \approx 1.7$ GeV comes from the contribution of the candidate $N'(1720)\ 3/2^+$. When removing it, the peak becomes a shoulder for the whole range of Q^2 analysed.

unpolarized resonant cross sections obtain additional contributions from the $S_{1/2}$ electrocouplings, to which $\Delta(1700)\ 3/2^-$ is the major contributor at $Q^2 > 2.0$ GeV^2 [55]. For this reason, the third resonance region becomes slightly enhanced as Q^2 increases, when compared to the transverse cross sections.

In Fig. 5, the total sum of all resonance contributions to the transverse, σ_T^R and unpolarized, σ_U^R virtual photon-proton cross sections is shown for an electron beam energy of 10.6 GeV, and compared with representative examples of unpolarized cross section data [15, 17]. Note that the CLAS F_2 data were extracted from the measured differential cross sections via the parametrization in Ref. [9] for the ratio $R_{LT}^{\rm old}$. We opt to use and updated version for $R_{LT}^{\rm new}$ as in Ref. [19], based on H1 and ZEUS data [20–22]. In order to do so, we use the interpolated $F_2^{\rm old}$ data [17], and transform them into the update version $F_2^{\rm new}$ via the appropriate relation

$$F_2^{\rm new} = \frac{R_{LT}^{\rm new}+1}{R_{LT}^{\rm old}+1}\frac{\epsilon_T R_{LT}^{\rm old}+1}{\epsilon_T R_{LT}^{\rm new}+1}F_2^{\rm old}. \qquad (14)$$

The unpolarized cross section data are transformed accordingly. Note that the choice of the new R_{LT} parametrization leads to a slight change in the unpolarized cross section data, especially in the second and third resonance regions and larger Q^2 bins. However, the difference is smaller than the 1σ theory bands.

We discussed above how the different resonances cluster into three regions, which correspond to the three peaks in W observed in the unpolarized cross sections. The transverse resonant part gives the largest contribution to the resonant cross sections. The size of the longitudinal part increases with W, but overall does not exceed 30% of the total cross section in the kinematical region shown in Fig. 5. Hence, the shapes of the resonant contributions to unpolarized and transverse cross sections are similar, and they both clearly show three separate peaks. The unpolarized resonant cross sections show a pronounced evolution with Q^2: both the first and the third regions show a stronger fall-off with Q^2 than the second peak. In particular, in the first region at $Q^2 = 1$ GeV^2, the resonant contribution is responsible for about 70% of the cross section; at $Q^2 = 4$ GeV^2 it accounts for less than 40%. However, in the second region the resonant contributions remain almost unchanged

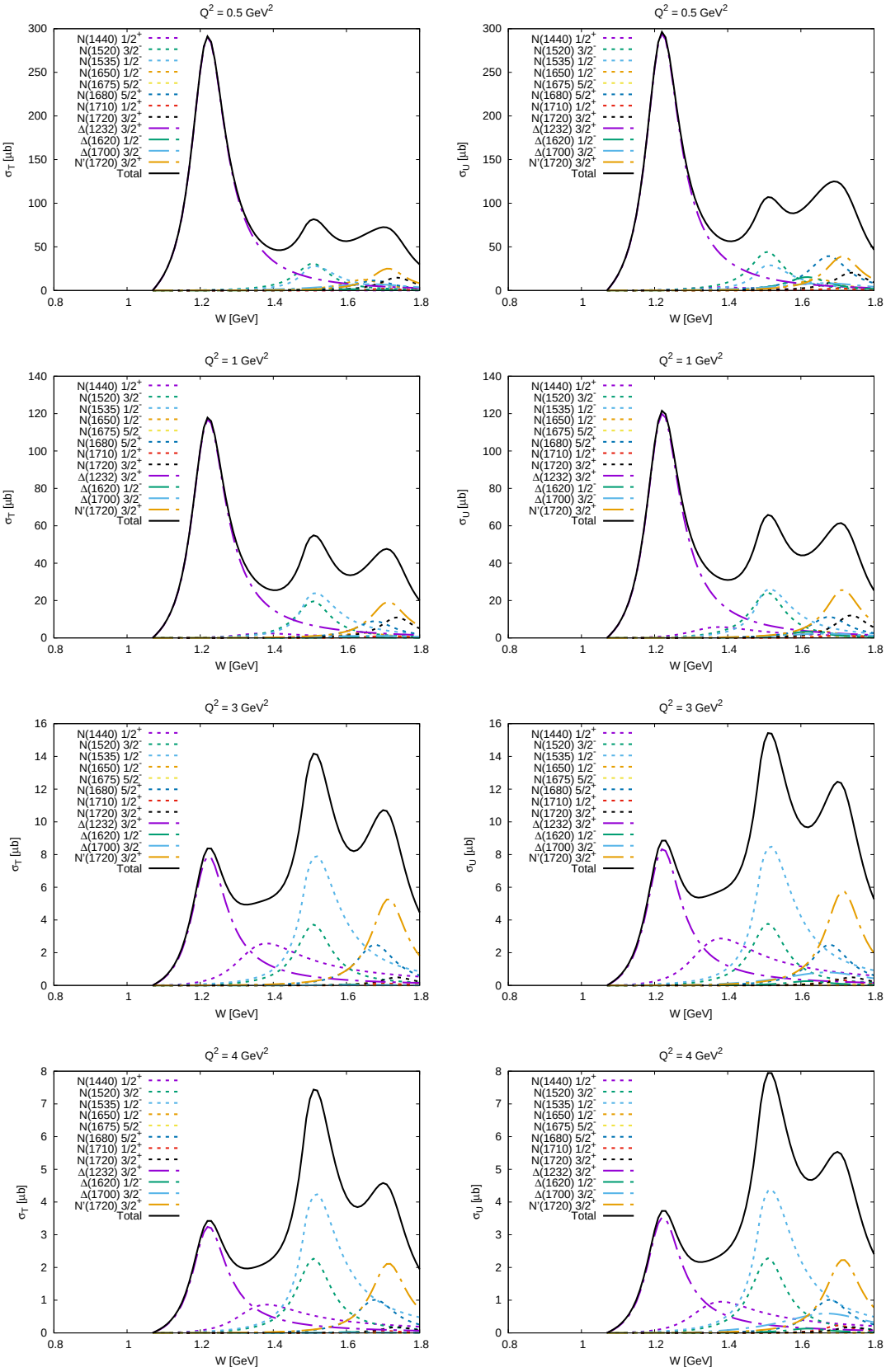

Figure 4. Decomposition of the transverse (thick black curves in the left column) and unpolarized (thick black curves in the right column) resonant cross sections into the separate contributions of each resonance included in the model at different representative Q^2, and at an electron beam energy of 10.6 GeV.

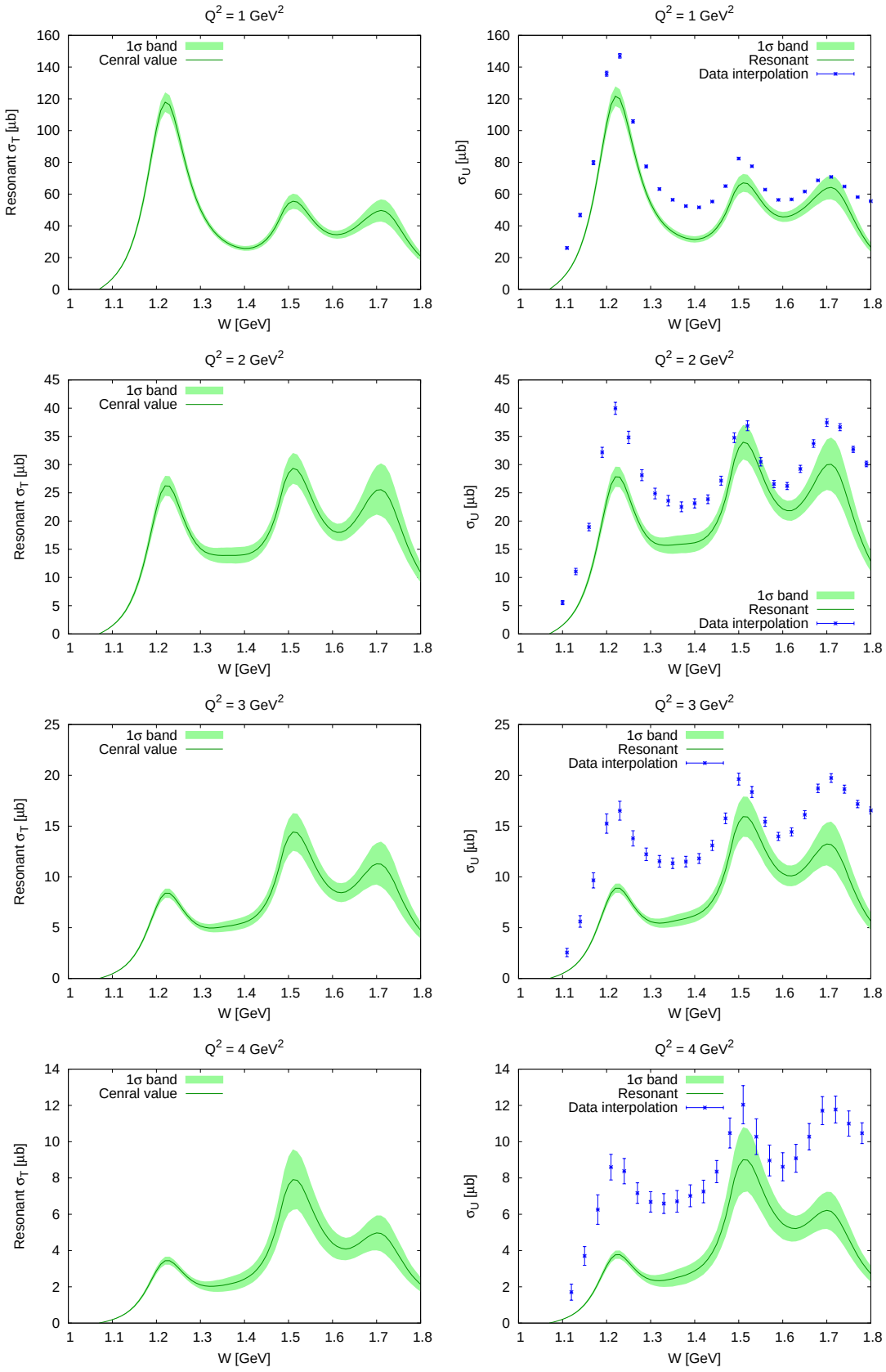

Figure 5. Resonant contributions (green curves with uncertainty bands) to the transverse σ_T (left column) and unpolarized σ_U (right column) virtual photon-proton cross sections. The unpolarized cross sections are presented for the electron beam energy 10.6 GeV, and the data points and error bars are obtained in [17] by interpolating the CLAS and world measurements as described in Ref. [15], with an updated version of R_{LT}, as described in the text.

with Q^2, at the level of 80%, mainly due to the slow evolution with Q^2 of the $N(1535)$ $1/2^-$ $A_{1/2}$ electrocoupling. In the third region, the resonant contribution decreases from 90 % to 50 % within the aforementioned Q^2 range. This suggests that the different excited nucleon states display distinctively different structural features in the Q^2 evolution of their electrocouplings, further underlining the results in Fig. 4. Therefore, in order to explore the strong QCD dynamics underlying the generation of the ground and excited nucleon states, the results on electrocouplings of all prominent nucleon resonances are needed.

In the future our results on the resonant longitudinal contributions could be compared to the longitudinal virtual photon-proton cross sections. These can be inferred from the Hall C data at Jefferson Lab on inclusive electron scattering cross sections [14, 74], which provide the information on the R_{LT} ratio. The knowledge of the resonant contributions to the longitudinal cross section offers new opportunities in accessing gluon distributions at x within the resonance region [75].

First experiments with the CLAS12 detector in Hall B at Jefferson Lab started in the Spring of 2018. The expected results will extend the available data on inclusive electron scattering in the resonance region to high photon virtualities of $Q^2 > 4.5$ GeV^2 [23]. The predicted virtual photon-proton cross sections based on the interpolation/extrapolation of the experimental results [17] and the resonant contributions estimated as described in Section II are shown in Fig. 6. The uncertainties are computed for the expected inclusive electron scattering event statistics collected in the Spring 2018 run of integrated luminosity 12.8 μb^{-1} [15], and for the kinematic grid bin sizes $\Delta W = 0.01$ GeV and $\Delta Q^2 = 0.1$ GeV^2. The expected statistical precision of the data is in the range from 0.2% to 2.0%, suggesting that the data uncertainties will be mostly determined by the measurement systematics. The computed resonant contributions allow us to elucidate the role of nucleon resonances in the measured inclusive electron scattering observables. The present paper thus offers a ready-to-use phenomenological tool for the analysis of the inclusive electron scattering data measured with CLAS12. This tool is available online [17], allowing the interactive evaluation of inclusive electron scattering observables together with resonant contributions computed for integrated luminosities and kinematics grids as defined by the user.

In our approach, the estimates for the resonant contributions are obtained from exclusive meson electroproduction data, which are independent from the inclusive electron scattering observables. This enables to evaluate the non-resonant contributions to inclusive electron scattering observables as the differences between the measured inclusive observables and the estimated resonant contributions. Of course, these estimates cannot duly isolate the interference terms between the resonant and non-resonant contributions for the exclusive channels. In Fig. 7, we show the thus obtained non-resonant contributions to the CLAS data on the inclusive structure function F_2 [9]. Unlike for the unpolarized cross sections, the choice of the new parametrization for R_{LT} is barely noticeable in the F_2 data, since this observable is not very sensitive to this ratio. Overall, bearing in mind the large number of resonances and opening channels present, the resulting non-resonant contributions are rather smooth functions of W, especially at higher Q^2. We compare the contributions inferred from the data with the background model from Ref. [11], which can be considered as the continuation of the background from the deep inelastic scattering region into the resonance region. The non-resonant contributions determined by realistically accounting for the nucleon resonances, as described in Section II, demonstrate several structures and a sharp increase at W from 1.6 GeV to 1.7 GeV seen in all Q^2-bins. One can observe several kinks in the W dependence of the background for F_2. It appears, however, that each of them is associated with the opening of a meson-baryon channel, namely $\pi\pi N$ at 1.21 GeV, ηN at 1.49 GeV, and ωN at 1.72 GeV. We also show the W-values for the opening of the $\pi^+N(1520)$ $3/2^-$, $\pi^+N(1680)$ $5/2^+$ and ρN channels, calculated at the resonance **central** masses. Because of the appreciable decay widths ($\gtrsim 100$ MeV) of the unstable final states, instead of kinks these channels produce sharp growths in the W dependence of the F_2 structure function at 1.6 GeV $\lesssim W \lesssim$ 1.7 GeV, seen in all Q^2 bins. All these features seen in the W dependence of the non-resonant contribution defined here are likely related to the manifestation of coupled channel effects.

IV. SUMMARY

In this work, we have developed a model for the evaluation of the resonant contributions to observables of inclusive electron scattering off protons. Due to the advances made by the exclusive reaction studies with CLAS [37, 42], we have experimental results on $\gamma_v pN^*$ electrocouplings of most of the excited nucleon states in the mass range below 1.8 GeV. For the first time, the resonant contributions to inclusive electron scattering observables have been evaluated from the experimental results on $\gamma_v pN^*$ resonance electrocouplings and the total decay widths. In particular, we computed the virtual photon and electron scattering cross sections and the F_2 structure function, at $W \leq 1.8$ GeV and 0.5 GeV$^2 \leq Q^2 \leq$ 6.0 GeV^2. Our approach allows for the separation of the resonant part into longitudinal and transverse contributions.

Our studies elucidate the contributions from excited nucleon states to the three resonance regions. We observed substantial contributions from the resonance tails in the neighboring regions. We found a nontrivial behaviour in the Q^2 evolution of the resonance structures: the first and third peaks decrease strongly with Q^2, not only in their absolute value, but also relatively to the background; on the other hand, the second region decreases with Q^2, but it stays relatively constant with re-

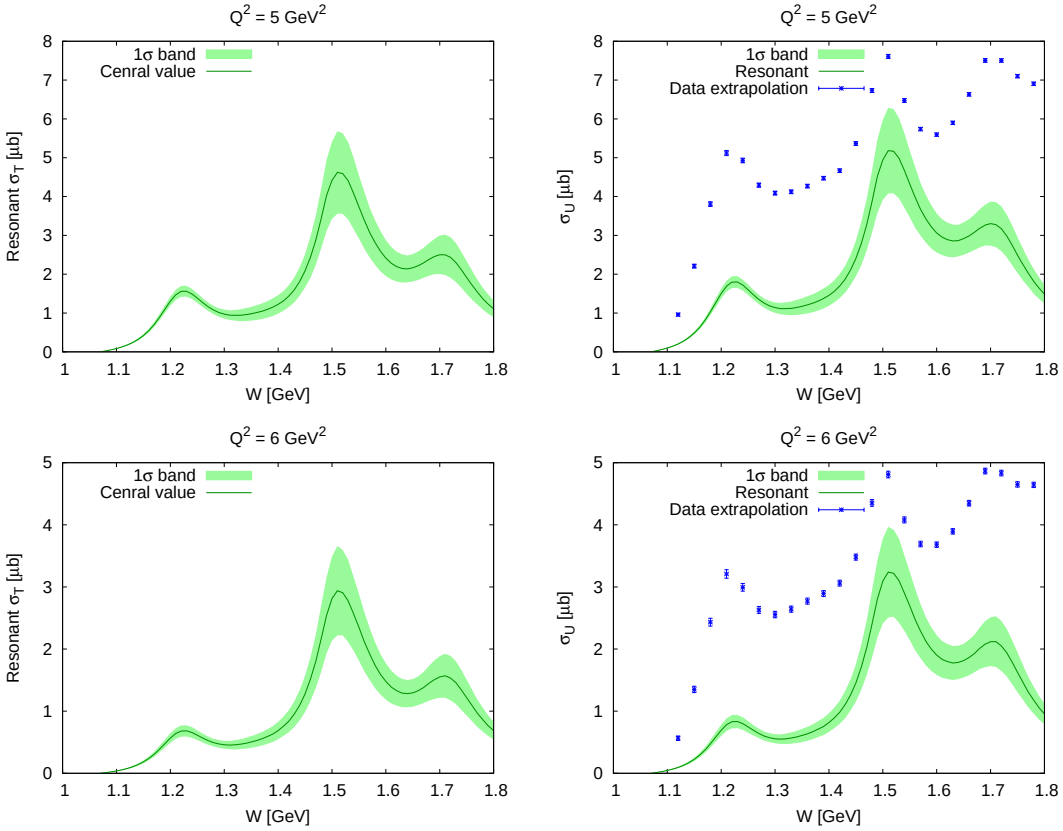

Figure 6. Predicted inclusive virtual photon-proton cross sections (points with error bars) and resonant contributions at $Q^2 = 5.0$ GeV^2 (top) and $Q^2 = 6.0$ GeV^2 (bottom) in the kinematic area covered in the measurements with the CLAS12 detector [23]. The error bars for the projected data shown in the plot are obtained for the statistics corresponding to the integrated luminosity collected with CLAS12 in the Spring 18 run and bin sizes $\Delta W = 0.01$ GeV and $\Delta Q^2 = 0.1$ GeV^2. Further explanations as in Fig. 5.

spect to the background. Such a behaviour underlines the essential differences in the structure of the excited nucleon states in the three regions. Studies of the $\gamma_v pN^*$ electrocouplings of all prominent nucleon resonances offer a unique way to explore the many facets of strong QCD in the generation of excited nucleons of different quantum numbers with distinctively different structural features.

By comparing the resonant contributions to the F_2 data from CLAS [9], we are therefore able to extract the separate contribution of the background as the difference between data on F_2 inclusive structure functions and the resonant contributions. The thus evaluated background shows several kinks and a sharp increase at W from 1.6 GeV to 1.7 GeV in all Q^2 bins covered by the CLAS data. This is related to the opening of different meson-baryon channels contributing to inclusive observables.

We aim to use this work as a benchmark for describing low and high-energy data in wide Q^2 regions with one single combined resonance-background model. This is motivated by the CLAS12 experiments on both exclusive and inclusive electron-induced reactions, which will extend the data base for comparison and constraints on the model towards high photon virtualities of $Q^2 > 4.5$ GeV^2.

ACKNOWLEDGMENTS

The authors thank I. G. Aznauryan, W. Melnitchouk, J. Qiu, and Ch. Weiss for their valuable input. This material is based upon work supported by the U.S. Department of Energy, Office of Science, Office of Nuclear Physics under contracts DE-AC05-06OR23177 and DE-FG02-87ER40365, U.S. National Science Foundation under Grants No. PHY-1415459 and No. PHY-1513524, PAPIIT-DGAPA (UNAM, Mexico) under Grant No. IA101819, CONACYT (Mexico) under Grant No. 251817, Deutsche Forschungsgemeinschaft (DFG) project "SFB 1044, Teilprojekt S2", and the Skobeltsyn Nuclear Physics Institute and Physics Department at Moscow State University.

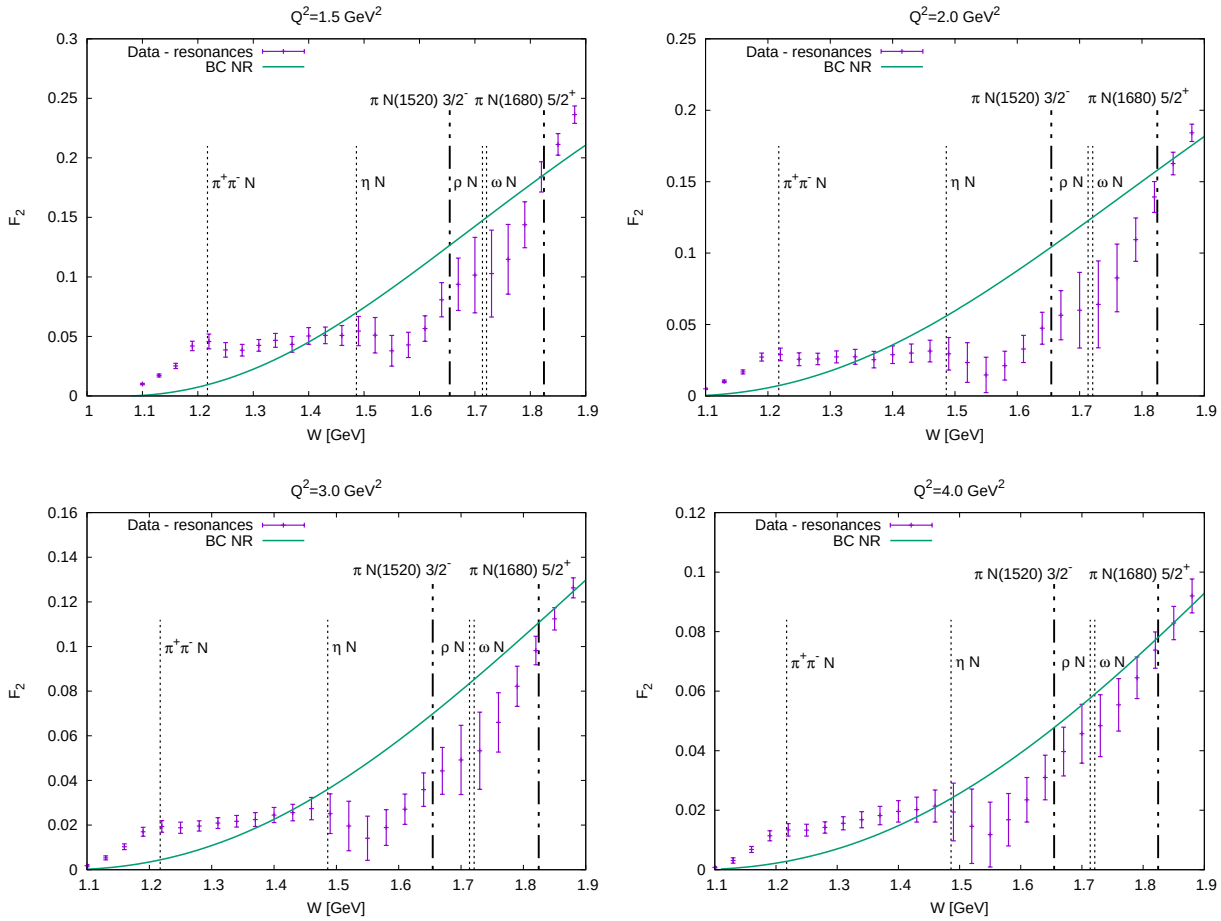

Figure 7. Results (purple points with error bars) on the differences between the F_2 structure functions estimated by interpolating the CLAS/world results [15, 17] and the estimated resonant contributions, compared to the background as in Ref. [11] (green curve). The dotted vertical lines show the opening of meson-nucleon electroproduction channels. The dash-dotted vertical lines show the opening of π N^* channels. The data and model uncertainties are propagated into the final error bars shown. The green curve is the background (NR) as in the model of Ref. [11] (BC), which can be considered as the continuation of the background from the deep inelastic scattering region into the resonance region.

[1] L. A. Harland-Lang, A. D. Martin, P. Motylinski, and R. S. Thorne, Eur. Phys. J. **C75**, 204 (2015), arXiv:1412.3989 [hep-ph].

[2] S. Dulat, T.-J. Hou, J. Gao, M. Guzzi, J. Huston, P. Nadolsky, J. Pumplin, C. Schmidt, D. Stump, and C. P. Yuan, Phys. Rev. **D93**, 033006 (2016), arXiv:1506.07443 [hep-ph].

[3] A. Accardi, L. T. Brady, W. Melnitchouk, J. F. Owens, and N. Sato, Phys. Rev. **D93**, 114017 (2016), arXiv:1602.03154 [hep-ph].

[4] S. Alekhin, J. Blümlein, S. Moch, and R. Placakyte, Phys. Rev. **D96**, 014011 (2017), arXiv:1701.05838 [hep-ph].

[5] R. D. Ball *et al.* (NNPDF Collaboration), Eur. Phys. J. **C77**, 663 (2017), arXiv:1706.00428 [hep-ph].

[6] P. Jimenez-Delgado, W. Melnitchouk, and J. F. Owens, J. Phys. **G40**, 093102 (2013), arXiv:1306.6515 [hep-ph].

[7] J. Gao, L. Harland-Lang, and J. Rojo, Phys. Rept. **742**, 1 (2018), arXiv:1709.04922 [hep-ph].

[8] A. Deur, S. J. Brodsky, and G. F. De Téramond, (2018), arXiv:1807.05250 [hep-ph].

[9] M. Osipenko *et al.* (CLAS Collaboration), Phys. Rev. **D67**, 092001 (2003), arXiv:hep-ph/0301204 [hep-ph].

[10] S. P. Malace *et al.* (Jefferson Lab E00-115 Collaboration), Phys. Rev. **C80**, 035207 (2009), arXiv:0905.2374 [nucl-ex].

[11] M. E. Christy and P. E. Bosted, Phys. Rev. **C81**, 055213 (2010), arXiv:0712.3731 [hep-ph].

[12] Y. Prok *et al.* (CLAS Collaboration), Phys. Rev. **C90**, 025212 (2014), arXiv:1404.6231 [nucl-ex].

[13] C. E. Keppel, M. I. Niculescu, *et al.*, (2000), JLab experiment E00-002.

[14] Y. Liang *et al.* (Jefferson Lab Hall C E94-110 Collaboration), (2004), arXiv:nucl-ex/0410027 [nucl-ex].

[15] A. A. Golubenko, V. V. Chesnokov, B. S. Ishkhanov, and

V. I. Mokeev, (2019), arXiv:1902.02900 [hep-ex].
[16] "CLAS Physics Database," https://clasweb.jlab.org/physicsdb/.
[17] "Structure functions and cross-sections Database," http://clas.sinp.msu.ru/strfun/.
[18] G. Ricco, S. Simula, and M. Battaglieri, Nucl. Phys. **B555**, 306 (1999), arXiv:hep-ph/9901360 [hep-ph].
[19] O. Tomalak and M. Vanderhaeghen, Eur. Phys. J. **C76**, 125 (2016), arXiv:1512.09113 [hep-ph].
[20] L. W. Whitlow, S. Rock, A. Bodek, E. M. Riordan, and S. Dasu, Phys. Lett. **B250**, 193 (1990).
[21] S. Dasu *et al.*, Phys. Rev. **D49**, 5641 (1994).
[22] M. Arneodo *et al.* (New Muon Collaboration), Nucl. Phys. **B483**, 3 (1997), arXiv:hep-ph/9610231 [hep-ph].
[23] V. D. Burkert, Ann. Rev. Nucl. Part. Sci. **68**, 405 (2018).
[24] R. P. Feynman, Conf. Proc. **C720611**, 75 (1972).
[25] G. R. Farrar and D. R. Jackson, Phys. Rev. Lett. **35**, 1416 (1975).
[26] F. E. Close and A. W. Thomas, Phys. Lett. **B212**, 227 (1988).
[27] E. Leader, A. V. Sidorov, and D. B. Stamenov, Eur. Phys. J. **C23**, 479 (2002), arXiv:hep-ph/0111267 [hep-ph].
[28] E. R. Nocera, Phys. Lett. **B742**, 117 (2015), arXiv:1410.7290 [hep-ph].
[29] X. Ji, Phys. Rev. Lett. **110**, 262002 (2013), arXiv:1305.1539 [hep-ph].
[30] A. V. Radyushkin, Phys. Rev. **D96**, 034025 (2017), arXiv:1705.01488 [hep-ph].
[31] Y.-Q. Ma and J.-W. Qiu, Phys. Rev. Lett. **120**, 022003 (2018), arXiv:1709.03018 [hep-ph].
[32] H.-W. Lin *et al.*, Prog. Part. Nucl. Phys. **100**, 107 (2018), arXiv:1711.07916 [hep-ph].
[33] E. D. Bloom and F. J. Gilman, Phys. Rev. Lett. **25**, 1140 (1970).
[34] W. Melnitchouk, (2005), JLAB-THY-06-459.
[35] W. Melnitchouk, R. Ent, and C. Keppel, Phys. Rept. **406**, 127 (2005), arXiv:hep-ph/0501217 [hep-ph].
[36] M. E. Christy and W. Melnitchouk, J. Phys. Conf. Ser. **299**, 012004 (2011), arXiv:1104.0239 [nucl-ex].
[37] I. G. Aznauryan and V. D. Burkert, Prog. Part. Nucl. Phys. **67**, 1 (2012), arXiv:1109.1720 [hep-ph].
[38] K. Park *et al.* (CLAS Collaboration), Phys. Rev. **C91**, 045203 (2015), arXiv:1412.0274 [nucl-ex].
[39] V. I. Mokeev, I. Aznauryan, V. Burkert, and R. Gothe, EPJ Web Conf. **113**, 01013 (2016), arXiv:1508.04088 [nucl-ex].
[40] V. I. Mokeev, Few Body Syst. **57**, 909 (2016), arXiv:1602.04160 [nucl-ex].
[41] V. D. Burkert and C. D. Roberts, Rev. Mod. Phys. **91**, 011003 (2019), arXiv:1710.02549 [nucl-ex].
[42] V. I. Mokeev (CLAS Collaboration), Few Body Syst. **59**, 46 (2018), arXiv:1801.09750 [nucl-ex].
[43] V. D. Burkert, V. I. Mokeev, and B. S. Ishkhanov, (2019), arXiv:1901.09709 [nucl-ex].
[44] I. G. Aznauryan, Phys. Rev. **C67**, 015209 (2003), arXiv:nucl-th/0206033 [nucl-th].
[45] V. I. Mokeev, V. D. Burkert, T.-S. H. Lee, L. Elouadrhiri, G. V. Fedotov, and B. S. Ishkhanov, Phys. Rev. **C80**, 045212 (2009), arXiv:0809.4158 [hep-ph].
[46] I. G. Aznauryan *et al.* (CLAS Collaboration), Phys. Rev. **C80**, 055203 (2009), arXiv:0909.2349 [nucl-ex].
[47] V. I. Mokeev *et al.* (CLAS Collaboration), Phys. Rev. **C86**, 035203 (2012), arXiv:1205.3948 [nucl-ex].
[48] V. I. Mokeev *et al.*, Phys. Rev. **C93**, 025206 (2016), arXiv:1509.05460 [nucl-ex].
[49] I. G. Aznauryan, "Private communication,".
[50] M. Dugger *et al.* (CLAS Collaboration), Phys. Rev. **C79**, 065206 (2009), arXiv:0903.1110 [hep-ex].
[51] E. Golovatch *et al.* (CLAS Collaboration), Phys. Lett. **B788**, 371 (2019), arXiv:1806.01767 [nucl-ex].
[52] R. Thompson *et al.* (CLAS Collaboration), Phys. Rev. Lett. **86**, 1702 (2001), arXiv:hep-ex/0011029 [hep-ex].
[53] H. Denizli *et al.* (CLAS Collaboration), Phys. Rev. **C76**, 015204 (2007), arXiv:0704.2546 [nucl-ex].
[54] M. M. Dalton *et al.*, Phys. Rev. **C80**, 015205 (2009), arXiv:0804.3509 [hep-ex].
[55] "Nucleon resonances electro- and photocouplings," https://userweb.jlab.org/∼mokeev/resonance_electrocouplings/.
[56] E. L. Isupov *et al.* (CLAS Collaboration), Phys. Rev. **C96**, 025209 (2017), arXiv:1705.01901 [nucl-ex].
[57] N. Markov, K. Joo, M. Ungaro, L. C. Smith, and V. Mokeev, Few Body Syst. **59**, 134 (2018).
[58] G. V. Fedotov *et al.* (CLAS Collaboration), Phys. Rev. **C98**, 025203 (2018), arXiv:1804.05136 [nucl-ex].
[59] A. Trivedi, Few Body Syst. **60** (2019), 10.1007/s00601-018-1471-y.
[60] J. J. Dudek and R. G. Edwards, Phys. Rev. **D85**, 054016 (2012), arXiv:1201.2349 [hep-ph].
[61] A. D'Angelo *et al.*, (2016), JLab experiment E12-16-010.
[62] "Fits of the resonances electrocouplings," https://userweb.jlab.org/∼isupov/couplings/.
[63] M. Tanabashi *et al.* (Particle Data Group Collaboration), Phys. Rev. **D98**, 030001 (2018).
[64] V. V. Frolov *et al.*, Phys. Rev. Lett. **82**, 45 (1999), arXiv:hep-ex/9808024 [hep-ex].
[65] C. S. Armstrong *et al.* (Jefferson Lab E94014 Collaboration), Phys. Rev. **D60**, 052004 (1999), arXiv:nucl-ex/9811001 [nucl-ex].
[66] G. Laveissiere *et al.* (JLab Hall A Collaboration), Phys. Rev. **C69**, 045203 (2004), arXiv:nucl-ex/0308009 [nucl-ex].
[67] N. F. Sparveris *et al.* (OOPS Collaboration), Phys. Rev. Lett. **94**, 022003 (2005), arXiv:nucl-ex/0408003 [nucl-ex].
[68] J. J. Kelly *et al.*, Phys. Rev. **C75**, 025201 (2007), arXiv:nucl-ex/0509004 [nucl-ex].
[69] S. Stave *et al.* (A1 Collaboration), Phys. Rev. **C78**, 025209 (2008), arXiv:0803.2476 [hep-ex].
[70] A. N. Villano *et al.*, Phys. Rev. **C80**, 035203 (2009), arXiv:0906.2839 [nucl-ex].
[71] L. Tiator, D. Drechsel, S. S. Kamalov, and M. Vanderhaeghen, Eur. Phys. J. ST **198**, 141 (2011), arXiv:1109.6745 [nucl-th].
[72] I. G. Aznauryan and V. D. Burkert, Phys. Rev. **C85**, 055202 (2012), arXiv:1201.5759 [hep-ph].
[73] V. I. Mokeev and I. G. Aznauryan, Int. J. Mod. Phys. Conf. Ser. **26**, 1460080 (2014), arXiv:1310.1101 [nucl-ex].
[74] V. Tvaskis *et al.*, Phys. Rev. **C97**, 045204 (2018), arXiv:1606.02614 [nucl-ex].
[75] G. Altarelli and G. Martinelli, Phys. Lett. **76B**, 89 (1978).